



## SIRIUS-T Structural System Design and Analysis

J.W. Powers, E.G. Lovell, I.N. Sviatoslavsky, R.L. Engelstad

October 1990

UWFDM-834

Presented at the 9th Topical Meeting on the Technology of Fusion Energy, 7-11 October  
1990, Oak Brook IL.

***FUSION TECHNOLOGY INSTITUTE***

***UNIVERSITY OF WISCONSIN***

***MADISON WISCONSIN***

### **DISCLAIMER**

This report was prepared as an account of work sponsored by an agency of the United States Government. Neither the United States Government, nor any agency thereof, nor any of their employees, makes any warranty, express or implied, or assumes any legal liability or responsibility for the accuracy, completeness, or usefulness of any information, apparatus, product, or process disclosed, or represents that its use would not infringe privately owned rights. Reference herein to any specific commercial product, process, or service by trade name, trademark, manufacturer, or otherwise, does not necessarily constitute or imply its endorsement, recommendation, or favoring by the United States Government or any agency thereof. The views and opinions of authors expressed herein do not necessarily state or reflect those of the United States Government or any agency thereof.

# **SIRIUS-T Structural System Design and Analysis**

J.W. Powers, E.G. Lovell, I.N. Sviatoslavsky, R.L.  
Engelstad

Fusion Technology Institute  
University of Wisconsin  
1500 Engineering Drive  
Madison, WI 53706

<http://fti.neep.wisc.edu>

October 1990

UWFDM-834

Presented at the 9th Topical Meeting on the Technology of Fusion Energy, 7–11 October 1990, Oak Brook IL.

## SIRIUS-T STRUCTURAL SYSTEM DESIGN AND ANALYSIS

J.W. Powers, E.G. Lovell, I.N. Sviatoslavsky, R.L. Engelstad  
Fusion Technology Institute  
University of Wisconsin-Madison  
1500 Johnson Drive  
Madison, WI 53706  
(608) 263-2352

### ABSTRACT

Structural integrity issues are addressed for a symmetric illumination laser driven tritium production facility. At critical locations in the reaction chamber's skeletal frame, mechanical stresses and deflections from self-weight loading are evaluated by finite element methods. Thermal stress analyses of the tiles constituting the chamber's first wall include a comparison of the response of carbon/carbon composite and graphite as well as the influence of irradiation. The results substantiate a viable design for the principal aspects of the reaction chamber.

### INTRODUCTION

SIRIUS-T is the conceptual design of a KrF laser driven ICF tritium production facility. Symmetric illumination of single shell targets is achieved with 92 radial beams which are positioned almost uniformly throughout the chamber as shown in Figure 1. The chamber is comprised of a V-3Ti-1Si vanadium alloy frame in the form of a reticulated shell (Figure 2) and removable tapered blanket modules which occupy the cells. The modules have hexagonal and pentagonal configurations with beam ports running through their centers. This configuration was motivated by the need for a large number of nearly identical planar geometric units (on the order of 100), to constitute the equivalent of the ideal spherical shape. The design is based upon icosahedron projections. The number of pentagonal modules is 12, which originates with the locations of the 12 vertices of the virtual regular icosahedron inscribed within the spherical surface. Each of the 20 triangular face projections of the icosahedron on the sphere can be uniformly subdivided into unique totals of identical hexagons, e.g., 30, 80, 150, etc. Such divisions are shown in Figure 3.<sup>1</sup> The beam number objective can be satisfied with the 12 pentagonal and 80 hexagonal units.

The modules are vanadium alloy canisters containing beryllium disks for neutron multiplication and liquid lithium as a breeder/coolant. The module surface facing the chamber center is covered by a protective graphite tile. Together these form the 4 m radius first surface of the facility. In the work which follows, results are presented

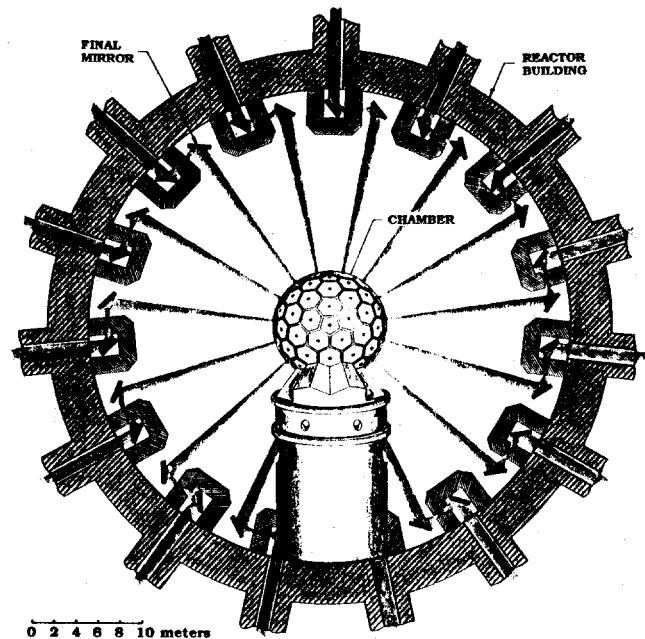


Figure 1. SIRIUS-T reactor chamber and containment building.

for an assessment of the structural integrity of the frame. The thermal stress analysis and design of the first surface tiles will also be described. Additional details of the overall characteristics of SIRIUS-T can be found in a companion paper.<sup>2</sup>

### FRAME STRUCTURAL ANALYSIS

The mechanical loads considered on the structural frame include the dynamic impulsive pressure which follows target implosion and the static dead weight load from the modules, coolant and frame itself. It has been determined that the pressure load resulted in negligible dynamic stresses and displacements of the frame. Typically, stresses did not exceed 10 MPa. Therefore, the investigation focused on evaluating the structural integrity of the frame from dead weight.

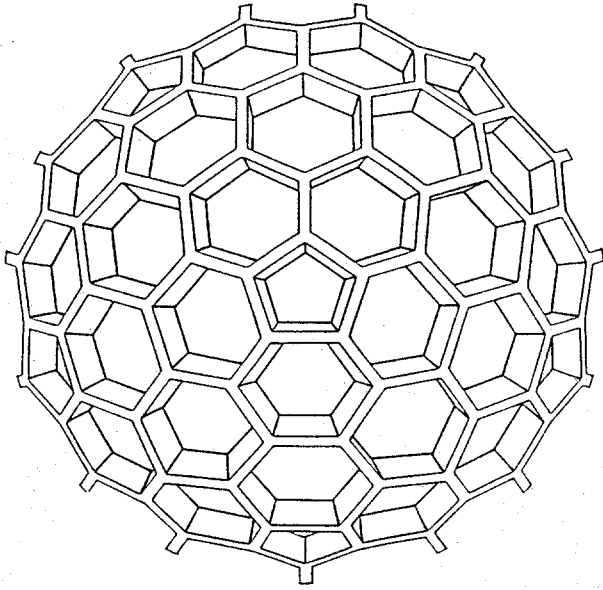


Figure 2. Reactor chamber structural frame with all modules removed.

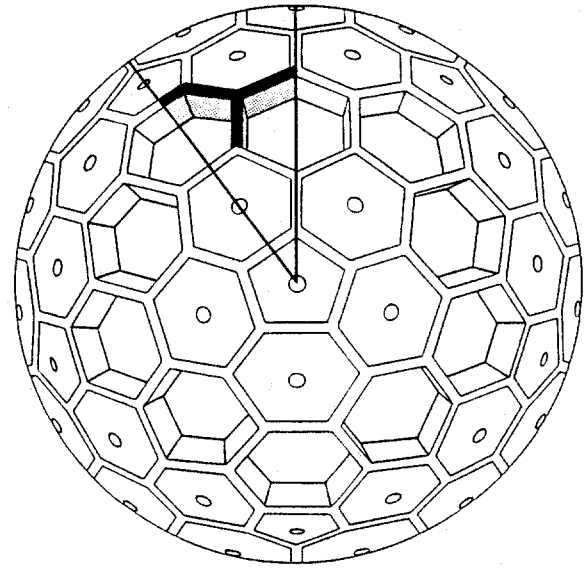


Figure 4. Bottom view of chamber with ten modules removed.

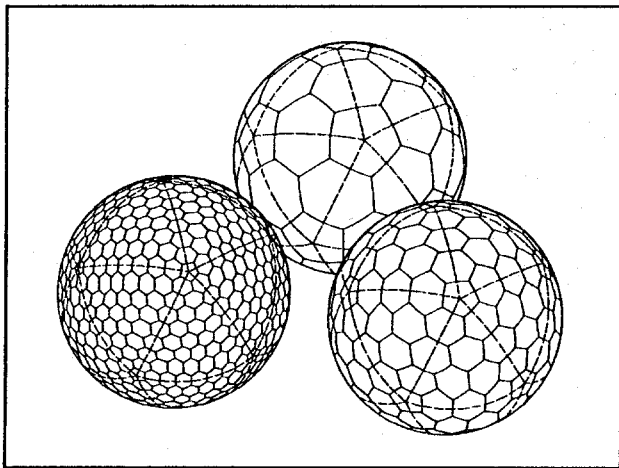


Figure 3. Icosahedron projections on spherical surfaces with different dividing frequencies.

A worst case scenario was proposed for the static loading. This consisted of removing the row of modules directly above the support pedestal, with all other modules kept intact. This is depicted in Figure 4, a bottom view in which the pedestal is not shown. Without this row of modules, the exposed supporting webs directly above the pedestal are subjected to the greatest dead weight load. The problem is exacerbated because this location also corresponds to the smallest number of webs to carry the load. At this position, webs are also inclined at the shallowest meridional angle, a geometric disadvantage which generally results in load magnification. A major issue is the determination of whether the webs could provide the necessary margin of strength and stiffness

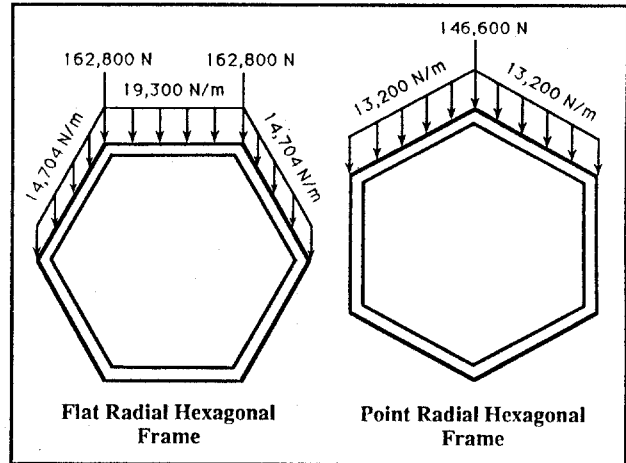


Figure 5. In-plane loading of a cell from dead weight.

under the most extreme conditions. Stresses should be within the yield strength design limits; stiffness should be sufficient to preclude web buckling as well as limit deflections to tolerances which would facilitate replacement of the modules for maintenance purposes.

To efficiently perform a structural analysis of the supporting frame, the symmetry of the module configuration was exploited. The row of modules removed alternates with "flat hexagonal" and "point hexagonal" cells around the perimeter. As previously mentioned, the dead weight loading on these cells is due to the frame and modules above. These loads are proportioned to the two types of cells in the form of both concentrated loads and

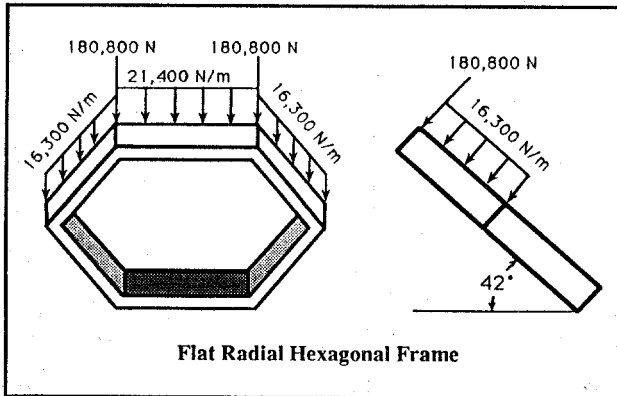


Figure 6. Out-of-plane loading of flat radial cell.

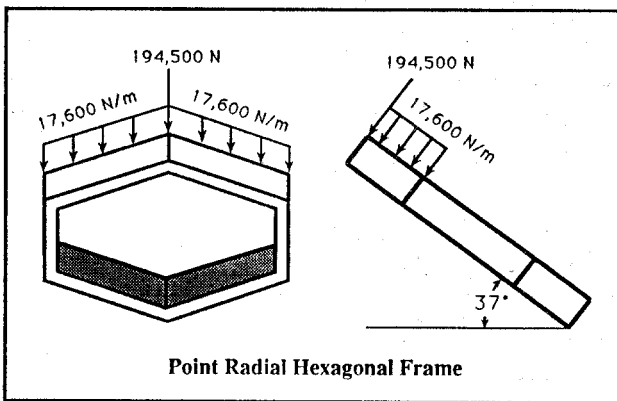


Figure 7. Out-of-plane loading of point radial cell.

distributed loads, as shown in Figures 5-7. The distributed loads are from the modules on the layer directly above and represent the actual load on the common web between individual modules and cells. Because the orientation of the frame varies at each layer of modules, it is necessary to differentiate the loads as either in-plane (Figure 5) or out-of-plane (Figures 6-7). In addition, the two types of cells differ slightly in the angle they make with the horizontal, i.e.,  $37^\circ$  versus  $42^\circ$  as shown in Figures 6 and 7. With the self-weight loads prescribed, a structural analysis of the exposed webs could be performed.

With the inherent symmetry of this structure, it was only necessary to analyze a representative subsection. The shaded portion of the frame in Figure 4 shows the section that was modeled with finite elements. It should be noted that this subsection consists of half of a "flat hexagonal" cell and half of a "point hexagonal" cell. This portion of the frame replicates itself exactly, or in a mirror image, around the perimeter of the chamber. The corresponding loads (concentrated only) and boundary conditions used for the finite element modeling are shown in Figure 8. By considering the various views of the figure, the exact orientation of the concentrated loads can be visualized, and

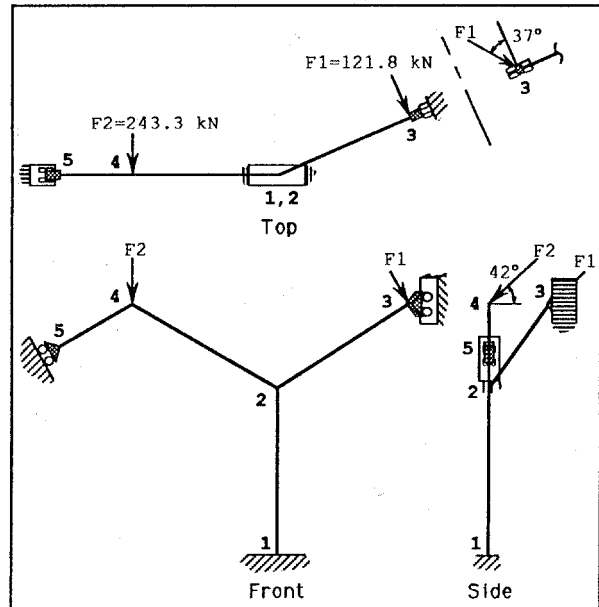


Figure 8. Loads, geometry and boundary conditions for finite element analysis.

the same methodology is used to apply the distributed loads. (Key node points are also noted on the structure.) It was assumed that the pedestal would provide essentially infinite rigidity to the lower webs that are in contact with it. Therefore, at node 1 the effective boundary condition is a rigid support with zero displacements and rotations, and there is no further need to consider these lower webs. The other boundary conditions shown in Figure 8 are due to symmetry constraints.

Material properties for unirradiated vanadium were used in the finite element computations, i.e., 124 GPa for the elastic modulus and 0.36 for Poisson's ratio.<sup>3</sup> It was assumed that the static loading for this particular case would take place during shutdown with a frame temperature of  $200^\circ\text{C}$ . Additional input data included the web dimensions, which were specified as 87 cm long by 80 cm deep by 8 cm thick. Finally, the commercial code ANSYS was used for all finite element calculations. Figure 9 shows a plot of the structural deflections from the applied loads (all displacements are exaggerated); actual displacement components at the key node points are given in Table 1. With the largest deflection of 1.754 mm at node 5, there should be no difficulty in replacing modules within the tolerance levels provided. Stresses were also well below the yield strength of the vanadium, i.e., less than 310 MPa. The location of the maximum tensile and compressive stress was at node 1, where the magnitudes were 70.1 MPa and -75.3 MPa, respectively.

A buckling analysis was also carried out for the structural webs. Results showed that stresses were far below critical values for elastic instability.

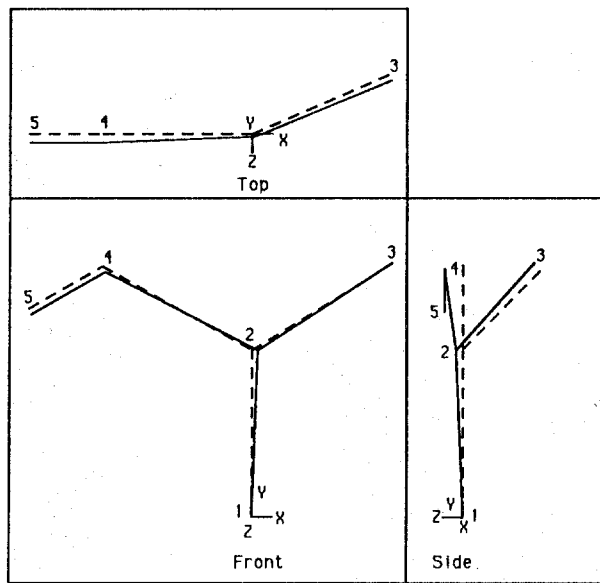


Figure 9. Displaced centerline of replicating unit.

Table 1. Displacement Components and Deflections (see Figure 8 for nodal locations)

Node	$\delta X$ (mm)	$\delta Y$ (mm)	$\delta Z$ (mm)	Total (mm)
1	0.000	0.000	0.000	0.000
2	0.484	-0.233	0.670	0.859
3	0.450	0.219	1.011	1.128
4	0.255	-0.463	1.622	1.706
5	0.333	-0.576	1.623	1.754

#### FIRST SURFACE THERMAL STRESS ANALYSIS

As shown in Figure 10, the blanket modules are protected by graphite tiles, which together form the near-spherical first surface of the facility. They operate with the back (blanket) side at a constant temperature of 960°K and receive intense short duration energy pulses on the front (cavity) side. With the tile thickness at 1 cm, deposition layers typically on the order of microns are essentially self-constrained from thermal expansion. Following target implosion, the temperature histories of the tiles are found from the code CONRAD,<sup>4</sup> with the effects of temperature-dependent conductivity included. This is input for a second code which numerically determines thermal stress, modeling the state as biaxial, isotropic and assessing the temperature dependence of the modulus, Poisson's ratio and the coefficient of thermal expansion.

The first tile material considered was a 4-D carbon/carbon composite developed by Fiber Materials, Inc.<sup>a</sup> Under intense thermal loads, such composites have

<sup>a</sup> FMI, Biddeford Industrial Park, Biddeford, ME, 04005

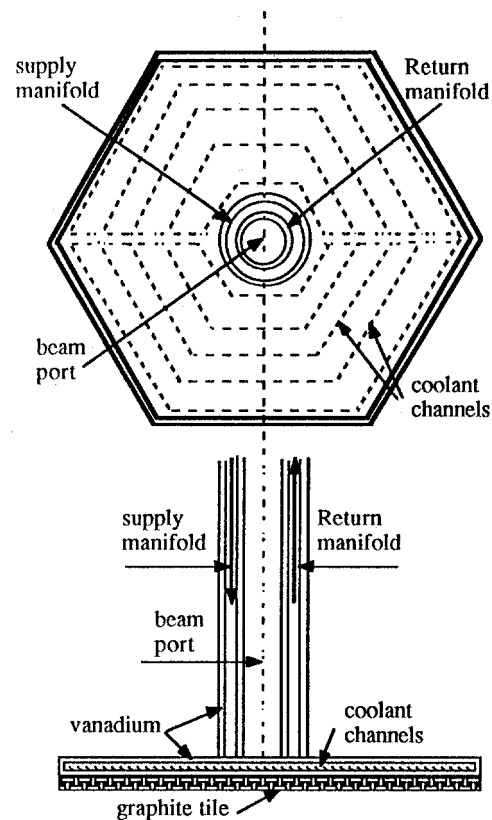


Figure 10. Blanket module with protective graphite tile.

shown higher resistance to crack growth than unreinforced graphite. The composites also have a natural porosity which enhances the material's capacity to accommodate thermal expansion. The temperature history for the unirradiated material is shown in Figure 11, with a maximum of 1449°K. The corresponding stress response of Figure 12 has a peak of 26.2 MPa, allowing for a safety factor of 2.1 when compared with strength at the corresponding temperature.

For comparison purposes, calculations were also made for H-451 graphite. This is a near isotropic, coarse-grained, extruded nuclear graphite developed for HTGRs. It was also selected because material properties are documented quite well.<sup>5</sup> For unirradiated material, the temperature and thermal stress histories of Figures 13 and 14 have maxima of 1488°K and 26.47 MPa, respectively. This corresponds to a strength safety factor of 2.5 at this temperature. Irradiation to  $10^{26}$  n/m<sup>2</sup> decreases the thermal conductivity at lower temperatures but does not appreciably change conductivity at temperatures from 1800 to 2300°K. The coefficient of thermal expansion is reduced, particularly at higher temperatures, while compressive strength and the modulus of elasticity increase after irradiation. In this case the maximum surface temperature rise is 1940°K and the thermal stress is higher as well at 49.6 MPa as indicated in Figures 15 and 16. However, the

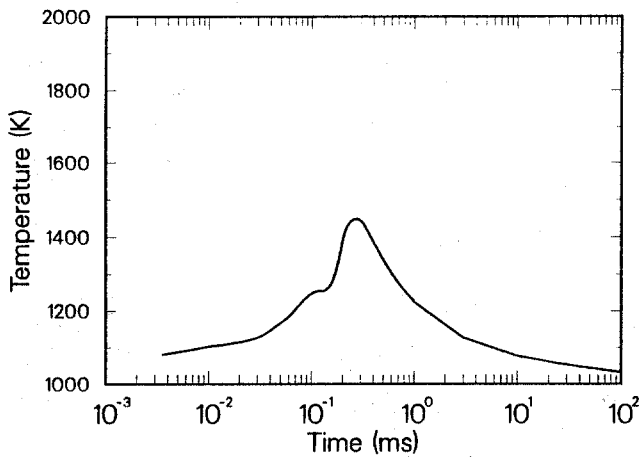


Figure 11. First surface temperature for unirradiated FMI carbon/carbon composite.

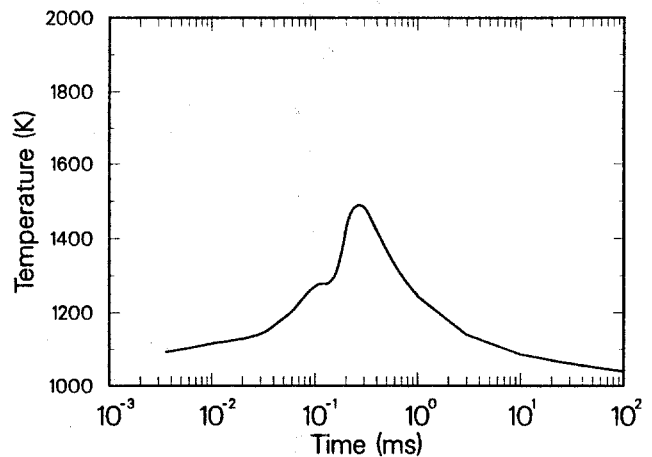


Figure 13. First surface temperature for unirradiated H-451 graphite.

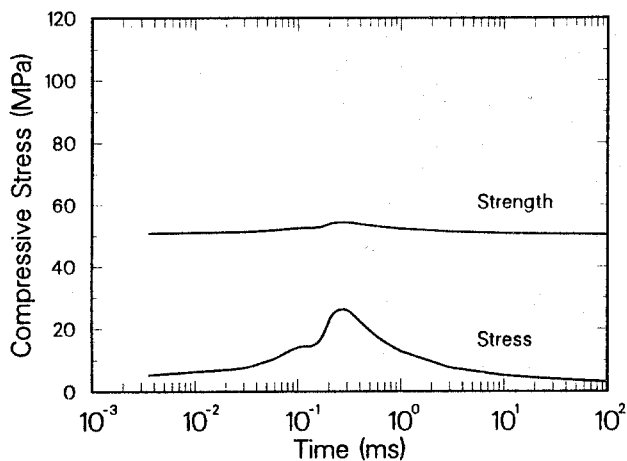


Figure 12. Thermal stress and strength for FMI composite tile.

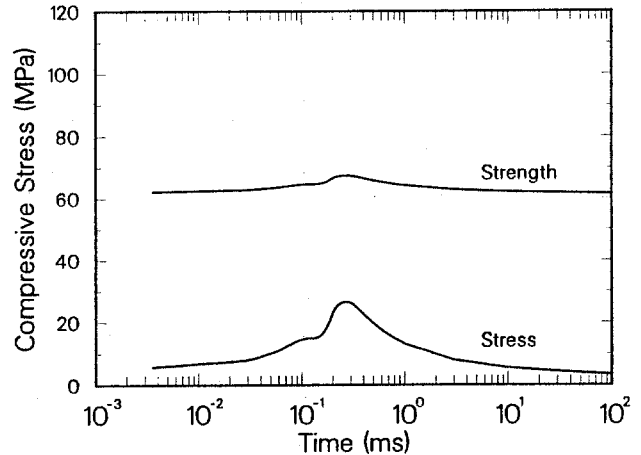


Figure 14. Thermal stress and strength for unirradiated H-451.

compressive strength is 94.4 MPa at this temperature and thus the safety factor is 1.9, not significantly different than the preceding cases. Irradiated strength rises with no increasing temperature to a maximum at about 1300°K and then begins to fall off. This causes the dip in the strength curve shown in Figure 16. In addition, representative temperature profiles for unirradiated graphite are shown in Figure 17. Curves (a) through (c) show the increasing gradient, reaching 1488°K at 0.252 ms. It can also be seen that the thickness of the heated/stressed layer is extremely small, typical for these cases.

## CONCLUSIONS

Results have been presented for stress and stiffness analyses of the structural frame of the SIRIUS-T reaction chamber. Computations were made by finite element methods for regions which are most highly loaded by dead weight of the frame, modules and liquid metal. Stresses were well below yield limits for the vanadium alloy V-3Ti-1Si. The frame is quite robust, resulting in high mechanical stiffness. Deflections of individual frame cells were sufficiently small to accommodate module removal and replacement without difficulty.

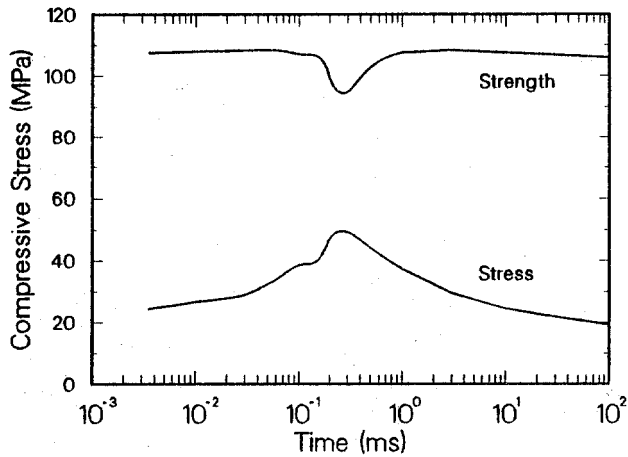


Figure 15. First surface temperature for irradiated H-451.

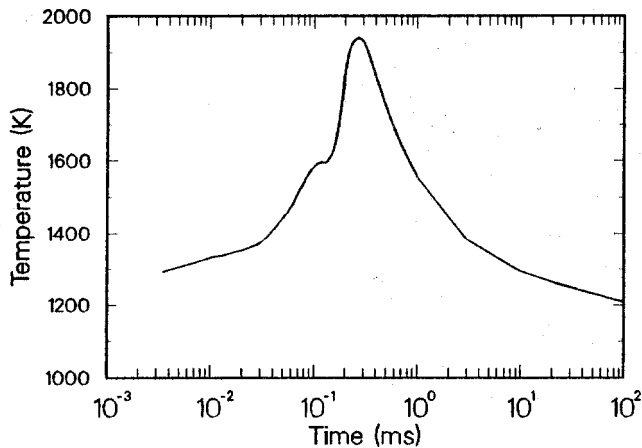


Figure 16. Thermal stress and strength for irradiated H-451.

A comparison was presented of the temperature and thermal stress response of first wall tiles of carbon/carbon composite, unirradiated and irradiated graphite. Variations in temperature-dependent and irradiation-dependent properties tended to be self-cancelling and resulted in peak thermal stresses that had practically the same margin of safety based upon mechanical strength.

The results substantiate the credibility of the structural design of the SIRIUS-T reaction chamber.

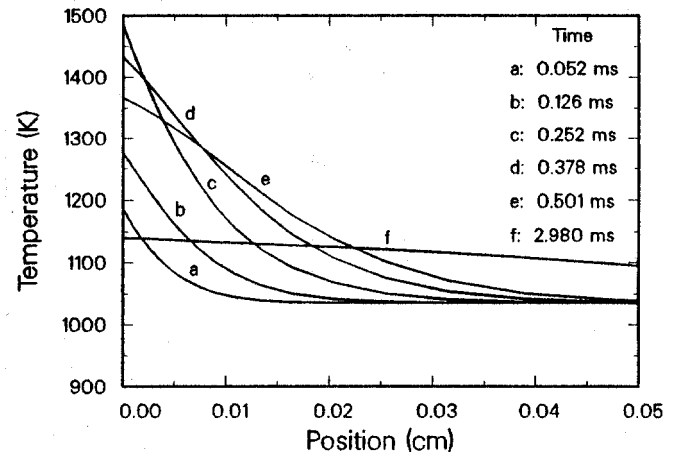


Figure 17. Temperature profiles in tiles of irradiated H-451.

#### ACKNOWLEDGEMENT

Support for this research has been provided by the Inertial Fusion Division, Office of Research and Advanced Technology, U.S. Department of Energy.

#### REFERENCES

1. R. DOERNACH, "Sphärische Raumfachwerke," *Der Stahlbau*, 29, 97 (1960).
2. I.N. SVIATOSLAVSKY, G.L. KULCINSKI, G.A. MOSES, M.E. SAWAN, R.L. ENGELSTAD, E.G. LOVELL, E. LARSEN, J.J. MacFARLANE, E. MOGAHED, R.R. PETERSON, J.W. POWERS, L.J. WITTENBERG, "SIRIUS-T - An Advanced Tritium Production Facility Utilizing Symmetrically Illuminated Inertial Confinement Fusion," these proceedings.
3. D.N. BRASKI, "The Post-Irradiated Tensile Properties and Microstructure of Several Vanadium Alloys," *ASTM-STP-1047* (1990).
4. R.R. PETERSON, J.J. MacFARLANE and G.A. MOSES, "CONRAD - A Combined Hydrodynamics-Condensation/Vaporization Computer Code," *UWFDM-670*, University of Wisconsin Fusion Technology Institute Report (1988).
5. G.R. HOPKINS et al., "Carbon and Silicon Carbide as First Wall Materials in Inertial Confinement Fusion Reactors," *GA-A14894*, General Atomic Co. Report (1978).